Cloud variability, radiative forcing and meridional temperature gradients in a general circulation model

By Peter L. Langen[1][*] and Rodrigo Caballero[2] ,

[1]*Centre for Ice and Climate, Niels Bohr Institute, University of Copenhagen, Copenhagen, Denmark;*
[2]*Meteorology and Climate Center, University College Dublin, Dublin, Ireland*

ABSTRACT

Due to the non-linearity of cloud-radiation interaction in general circulation models (GCMs), the time-mean cloud radiative forcing (CRF) is in general different from the CRF of time-mean clouds. This implies that a change in temporal cloud variability induces a change in radiative forcing even if there is no change in time-mean cloud properties. Here we investigate this variability contribution to CRF quantitatively in the NCAR CCM3.6 GCM. In a reference run, the variability contribution is found to account for 35% of the global-mean climatological CRF. The variability contribution peaks in the midlatitudes and is shown to be driven by synoptic eddy activity. In a climate change experiment, where the atmospheric CO_2 is quadrupled, the change in cloud variability offsets 40% of the change in CRF due to the change in mean clouds. It is found that almost all of this effect is due to variability in cloud fraction rather than in cloud water content, and it is traced to the non-linearity introduced by the model's treatment of vertical cloud overlap. This study indicates the possibility of an eddy variability-climate feedback that has not been extensively studied and quantified in the past.

1 Introduction

Clouds are observed to have a strong impact on Earth's radiative budget (Ramanathan et al., 1989). Cloud feedbacks can therefore exert potentially crucial influence on the climate system's response to external forcing, and may explain some outstanding features of ancient climates (Sloan and Pollard, 1998). However, the representation of cloud processes within general circulation models (GCMs) remains problematic, and is a leading source of uncertainty in estimates of climate sensitivity (Houghton et al., 2001; Bony et al., 2006). This reflects the almost overwhelming complexity of clouds and cloud-climate interaction (Randall et al., 2003; Stephens, 2005). The problem is rich enough that, despite several decades of research, many of its aspects have yet to be explored in detail.

The question of cloud-climate interaction in GCMs can be divided into two parts: one involving the way in which dynamics and thermodynamics create clouds, and the other concerning the way in which clouds interact with radiation and thus feed back on the thermodynamic and dynamic fields. Both are important, largely unsolved problems (Stephens, 2005). The scope of this paper falls into the second part; specifically, we analyze the variability effect of clouds on their time-mean radiative impact in the context of a particular GCM. A useful measure of cloud impact on radiative transfer is cloud radiative forcing (CRF), defined

as:

$$\mathrm{CRF} = R - R_{\mathrm{clr}}$$

where R is the total downward top-of-atmosphere radiative flux at a given longitude-latitude point, and R_{clr} is what R would be if clouds were instantaneously removed (which can be explicitly done in models; in observations, R_{clr} may be estimated from nearby clear-sky pixels). CRF is a non-linear function of cloud properties (Harshvardhan and Randall, 1985; Taylor and Ghan, 1992), and as a consequence, the time-mean CRF is not the same as CRF by time-mean clouds:

$$\overline{\mathrm{CRF}} = M(\overline{C}) + V(\overline{C}, C') \qquad (1)$$

where $\overline{()}$ represents a time average and $()'$ deviations therefrom, C collectively represents cloud properties in an atmospheric column, M is CRF due to time-mean clouds and V is the contribution to time-mean CRF due to temporal variability of clouds around the time mean.

As illustrated in Fig. 1, the non-linear dependence of CRF on C means that V is generally non-zero. It follows that a change in temporal cloud variability implies a change in radiative forcing even if clouds do not change in the mean. In the midlatitudes, cloud variability is driven mostly by synoptic eddy activity. A robust feature of GCM response to increased greenhouse forcing is a poleward shift of the midlatitude storm tracks accompanied by a change in eddy activity (Yin, 2005). There is thus the potential for a cloud variability-climate feedback that has not been extensively documented and quantified in the past.

This is not to imply that previous studies have disre-

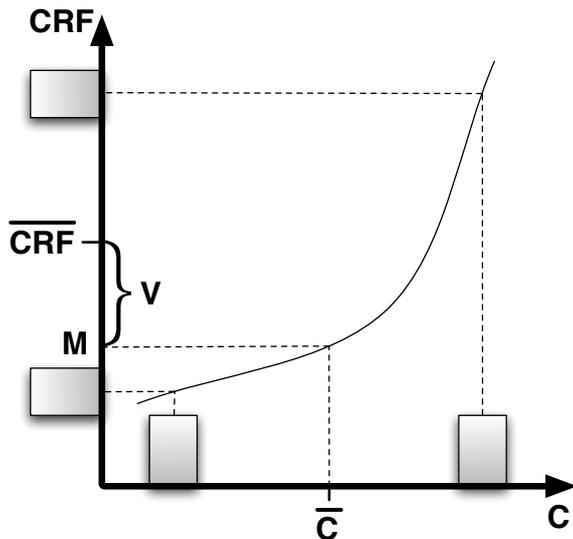[*] Corresponding author.
e-mail: plangen@gfy.ku.dk

Figure 1. Schematic illustrating the cloud variability effect. The bars on the C-axis denote the PDF of a simple form of variability, where the cloud properties attain only two values. The solid line illustrates a non-linear relationship between cloud properties and cloud radiative forcing, CRF. The bars on the CRF-axis give the PDF of the CRF resulting from the cloud distribution, and $\overline{\text{CRF}}$ shows the mean of this distribution. $\overline{C}$ is the mean of the cloud distribution and M is the CRF of this value. Due to the non-linearity of the relationship, there is a difference, V, between $\overline{\text{CRF}}$ and M.

garded the V contribution. There are two widely used methods to quantify cloud feedback, one employing offline radiative calculations (Wetherald and Manabe, 1988) and another (Cess and Potter, 1987; Cess et al., 1996) based on changes in CRF driven by surface temperature perturbations (see Soden et al., 2004, for a discussion of the relative merits of the two methods). Cloud variability is automatically included in the Cess et al. approach, while studies using the offline approach are careful to include the variability contribution by computing feedbacks as averages over a large ensemble of instantaneous radiative calculations. Thus, feedback values published in the literature all include contributions from both M and V.

What has been missing is a detailed study of the *partitioning* between M and V, and of the underlying causes of V. The main goal of this paper is to go some way towards filling this gap, albeit for a single GCM in a specific, simplified setup. In previous work (Alexeev et al., 2005; Caballero and Langen, 2005) we have examined the effect of changed eddy activity on dynamical poleward energy transport and changes in mean meridional temperature gradients. Here, we complement this earlier work by studying the effect of changed eddy activity on the meridional profile of cloud radiative forcing.

Some previous studies give an indication of the role played by V. Bergman and Salby (1997) used a single-column radiation model driven by observed cloud, temperature and humidity fields to diagnose the diurnal variability contribution to time-mean CRF, and found it could be as large as 20 W m^{-2}. Taylor and Ghan (1992), using an early version of NCAR's Community Climate Model (CCM1),

compared a climate change experiment in which cloud water content was held fixed to another in which it was allowed to vary in time. Clouds in both cases gave a negative (cooling) feedback to global warming, with cloud variability adding about 13% to this cooling. Using a GCM derived from the NCEP forecast model, Schneider et al. (1999) found that fixing cloud fraction and optical properties at their time-mean values led to a drop of up to 80 W m^{-2} in absorbed insolation when compared to a reference run with interactive clouds. Conversely, a similar experiment using GENESIS2 (Vavrus, 2004) showed that fixing clouds led to a warming of up to several degrees at high latitudes. These results show that V can be large and strongly model and climate state-dependent, and motivate further study.

The second aim of this paper is to identify the specific non-linearities that give rise to V. There are various candidates. One non-linearity is related to cloud water content: as the water content of a cloud increases from zero, the longwave emissivity first increases rapidly but then, past a certain threshold, the cloud becomes a black body and the emissivity becomes constant and equal to 1. The shortwave albedo behaves similarly, though with a different threshold. Thus, a cloud whose water content fluctuates from near zero to above-threshold values will have a strongly non-linear impact on both longwave and shortwave radiation.

Another important non-linearity is related to cloud overlap. The grid spacing in current GCMs is always much larger than individual clouds, so a cloudy grid cell will not in general be completely filled with cloud. Rather, the cloud parameterization predicts the fraction of the cell that is cloudy. This leaves the problem of how the cloudy fractions at different levels overlap. A variety of overlap schemes is used in current GCMs (Barker et al., 2003; Stephens et al., 2004). Among the simplest is the random overlap scheme, in which the horizontal disposition of cloud at one level is taken to be statistically independent from that at all other levels. As a result, the total cloud fraction c_{tot} is given by

$$c_{\text{tot}} = 1 - \prod_{i=1}^{N}(1 - c_i), \qquad (2)$$

where N is the total number of model levels and c_i is the cloud fraction at level i. The product term in this expression introduces an obvious non-linearity which will make itself felt when cloud fraction varies in time. As an example, consider the simplest case with only two cloudy layers. With cloud fraction constant at 0.5 in both layers, total cloudiness is $1 - (1 - 0.5)^2 = 0.75$. If instead the two layers vary in phase, with cloud fraction of 0 half the time and 1 the rest of the time, the time-mean total cloud cover is decreased to 0.5 without changing the mean value in each layer. Conversely, if the same variability is used in anti-phase the total cloud cover increases to 1. Thus, changes in cloud fraction variability can strongly affect CRF, the sign of the effect depending on the sign of the covariance between cloud fraction at different levels.

The random overlap method, first proposed by Manabe and Strickler (1964), is still in use in many modern GCMs; in particular, it is used in the longwave component of the GCM used here. Another commonly used method is the maximum-random scheme (Geleyn and Hollingsworth, 1979; Collins, 2001), in which adjacent cloud layers are maximally overlapped while layers separated by clear air are randomly

overlapped; the random component in this scheme introduces the same non-linearity discussed above. Yet another scheme (Briegleb, 1992) represents overlap effects by simply scaling the cloud layer optical depth by cloud fraction to the power 3/2, thereby introducing an explicit non-linear dependence on cloud fraction. An important point is that, for a given level of cloud fraction variability, each of these schemes will give a different CRF response. Thus, the cloud variability contribution to CRF is likely to be highly model dependent.

The plan of the paper is as follows. The model setup and the details of our CRF calculations are described in Section 2. In Sections 3 and 4, the role of V in the GCM is analyzed for the reference climate and a climate change experiment, respectively. Section 5 summarizes and concludes the study.

2   Model and methodology

The GCM employed in this study is the National Center for Atmospheric Research Community Climate Model (CCM) version 3.6.6 (Kiehl et al., 1996) with T21 horizontal resolution and 18 levels in the vertical. Keeping the experiment simple, we use an idealized model setup which simplifies the interpretation of the results: aquaplanet lower boundary conditions and an annually averaged diurnal cycle of solar forcing. This means that insolation and zenith angle have a diurnal cycle, but their daily-mean value is fixed and symmetric about the equator ("modified equinox" forcing; see Alexeev, 2003; Langen and Alexeev, 2004). We also exclude all effects of sea ice by fixing the surface albedo uniformly to 0.11 and treating subfreezing grid-points as open water. The solar constant has its current value of 1367 W m^{-2}.

We generated a reference climatology for this setup by setting CO_2 concentration at 355 ppm and running the model, coupled to a 50 m deep slab ocean, until sea surface temperatures (SSTs) had reached a statistically steady state. The model was then run for a further 20 years in this state to obtain the reference climatology, which has a global-mean SST of 15.3 °C and an equator-to-pole temperature gradient ($\sim 40K$) similar to that of the present-day northern hemisphere. This "realistic" temperature gradient was achieved in spite of the lack of high albedo surfaces at high latitudes by specifying a rather weak oceanic heat flux convergence corresponding to a maximum transport of only $0.5 \cdot 10^{15}$W.

To study the role of cloud variability in the reference run, we use an approach that is a hybrid between the offline radiative calculation method and the CRF method (see Section 1). It may be summarized in the following steps:

• The full GCM is run with SST fixed at the time-mean, zonal-mean value taken from the reference run. The 4 cloud properties that affect cloud-radiation interaction in this GCM (cloud fraction, cloud water content, effective radius and ice fraction) are output every 2 hours for 200 days.
• These cloud data are separated into time-mean and time-varying components: $C = \overline{C} + C'$, where C can represent any (or any combination) of the cloud parameters and synthetic datasets with any desired amplitude of variability are produced by scaling the variability component:

$$\tilde{C} = \overline{C} + q\,C'$$

with q a number between 0 and 1. Note that $\overline{\tilde{C}} = \overline{C}$ for all choices of q.
• The GCM is then re-run, again with fixed SST, but with prescribed cloud properties read from the synthetic dataset every 2 hours (linear interpolation is used for intervening time steps). These runs are 2 years long, looping over and reusing the 200-day cloud dataset.

The sensitivity of time-mean CRF in these fixed-SST runs to changes in q gives a quantitative measure of the role played by cloud variability in maintaining the climate of the reference run. A caveat of this method is that in the reference run, where clouds are fully interactive, the cloud and thermodynamic fields are closely correlated; this correlation is lost when using the resampled cloud data, and this can bias the CRF response, particularly in the longwave (Schneider et al., 1999). A further bias will be introduced by the use of fixed SST, but we expect this to be small since there is actually little SST variability in the reference run. We can quantify the overall bias by comparing the time-mean CRF of the reference run and the resampled run using $q=1$. As shown in the following section, the bias is very small (about 0.02 W m^{-2}) when compared to CRF changes induced by changing q. We thus feel confident that the method is accurate enough for the purposes of this study.

3   Cloud variability in the reference climate

The cloud resampling method described in the previous section is used here to ascertain the importance of the cloud variability contribution, V, to the total CRF in the reference climate of our model. For later reference, we first briefly examine some cloud statistics from the reference run. Fig. 2a presents time- and zonal-mean cloud fraction. The pattern in this figure compares well with those from GCM simulations of the modern climate, indicating that our idealized configuration is not in an unduly unrealistic regime. Cloud fraction variability (Fig. 2b) roughly follows the same pattern, with maxima at the equatorial tropopause, the low-level subtropics and the mid-troposphere in high latitudes. Cloud water content (not shown) shows a rather different pattern, with a large maximum in the time-mean at low levels over the equator, and a single, high-latitude variability maximum in each hemisphere.

Figs. 3a and b show the spectra of cloud fraction and vertical velocity (ω) at 35°N and 500 hPa determined from 200 day, two-hourly series. This is in the mid-latitude storm track region where the ω variance maximizes in the reference run. The plots both show a broad peak in the synoptic range centered at a period of approximately 5 days. Panel (c) shows the coherence (squared) spectrum of the two time-series. This quantity would be identically 1 at all frequencies for two linearly related, noise-free series and vanish for uncorrelated series. We see statistically significant coherence (with 99% confidence) in broad parts of the spectrum, especially around the synoptic time-scale. Clearly, the cloud fraction variability (and the radiative effects thereof, which will be studied here) is associated with vertical velocity fluctuations due to synoptic eddy variability.
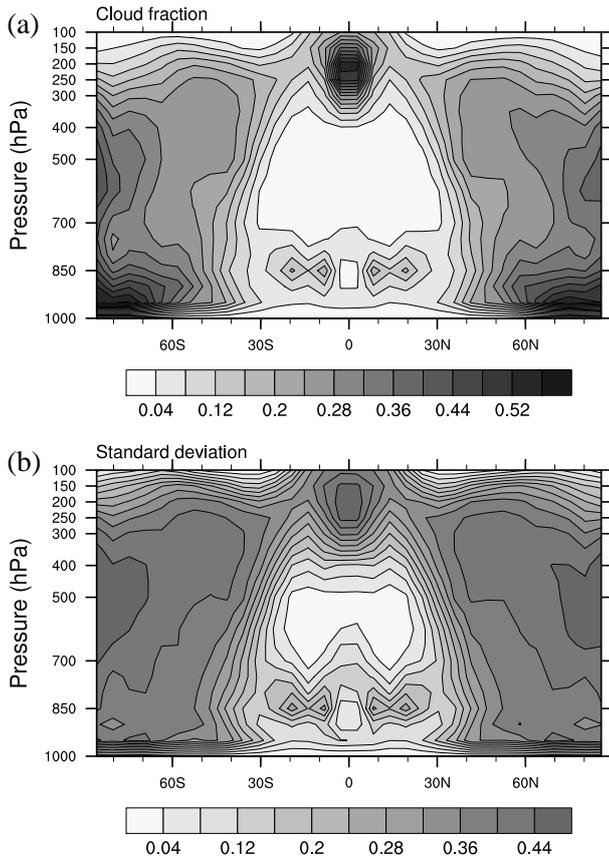
Figure 2. (a) Zonal-mean, time-mean cloud fraction and (b) zonal-mean standard deviation of cloud fraction in the reference run.
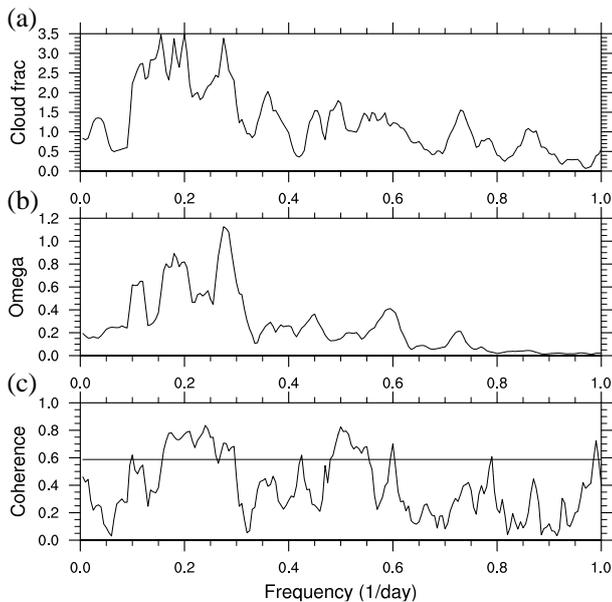

Figure 3. Spectra of 200 day, two-hourly series of (a) cloud fraction and (b) vertical velocity, ω, variability at 35°N and 500 hPa (arbitrary longitude). (c) Coherence spectrum of the two series. The straight line shows the coherence corresponding to the 99% level of confidence.
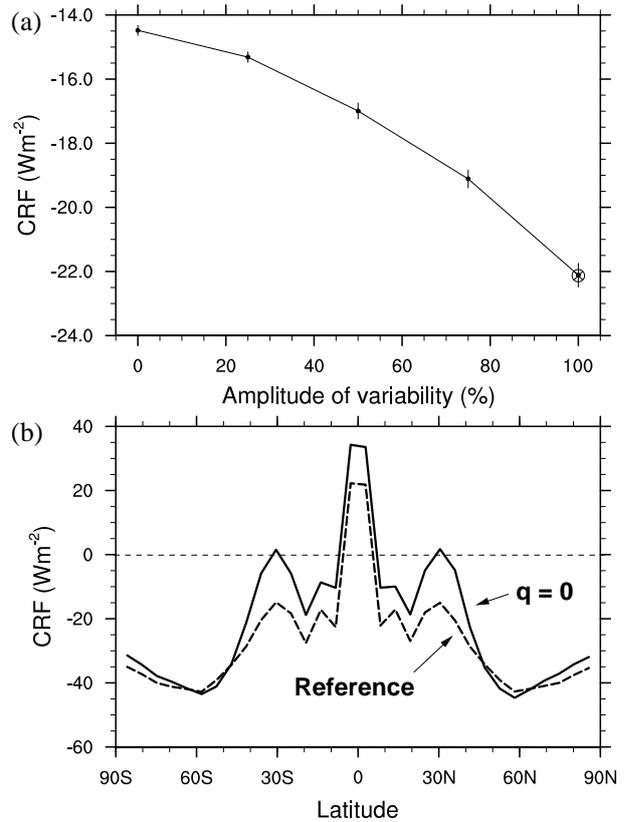

Figure 4. (a) Global average top-of-atmosphere CRF as function of scaling employed. Vertical bars denote one standard deviation over the two-year integration and the crossed-circle shows the case of internally calculated clouds. (b) Latitudinal structure of CRF with $q = 0$ (solid) and with internally calculated clouds (dashed).

Figure 4a shows the global average top-of-atmosphere CRF as a function of the variability amplitude, q. Time-mean clouds ($q=0$) give a global-mean CRF of about -14.5 W m^{-2}. This cooling tendency increases with increasing q, reaching -22.11 W m^{-2} when full cloud variability is used ($q=1$). The large crossed-circle symbol in the figure shows time- and global-mean CRF in the reference run, which has a value of about -22.13 W m^{-2}. The difference between this value and the $q=1$ fixed-SST value gives a measure of the bias inherent in our method, which is clearly very small. We conclude that, in this model, V, the variability contribution to CRF, plays a major role in the maintenance of the reference climate, accounting for about 8 W m^{-2} or 35% of total CRF.

These figures were obtained by scaling the variability in all cloud properties at the same time. Since the reference climate displays substantial variability in both cloud fraction and water content, it becomes interesting to determine the relative contributions of these variabilities to total CRF. This is addressed by conducting two additional fixed-SST runs, one with fixed cloud fraction and full water content variability, the other with these roles reversed. The two runs give a global-mean CRF of -14.8 and -22.7 W m^{-2}, respectively. Comparing these values with those in Fig. 4a, we see that cloud water content variability plays a negligible role. Furthermore, separate examination of short- and long-wave components of the water content contribution shows
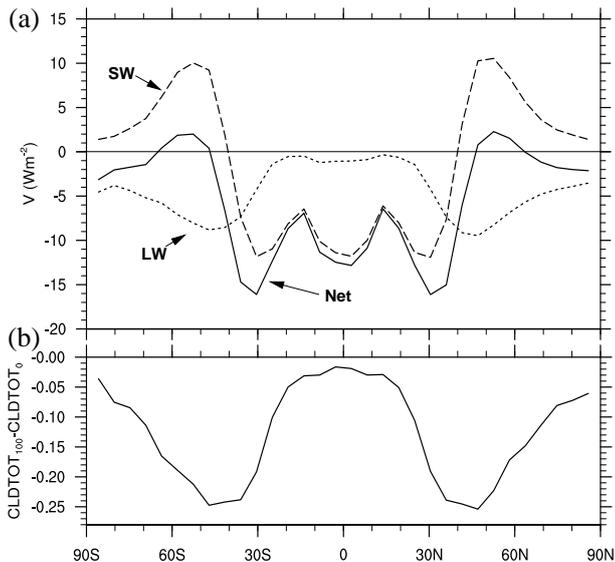
Figure 5. (a) Latitudinal structure of V (solid) in the reference run and shortwave (dashed) and longwave (dotted) contributions thereto. (b) The difference in vertically averaged (using random overlap) total cloud cover between the $q = 100\%$ and $q = 0\%$ runs.

that they are both small, so this is not a case of cancellation between two large but opposite quantities. This implies that the radiative scheme in the model has an approximately linear response to changes in cloud water content, at least over the range of values experienced in the present runs. Note, however, that a different cloud scheme or climate state may produce water content values in a range where the response is non-linear, so this result may not be robust.

Returning to our basic all-properties variability experiment, Fig. 4b compares the spatial structure of CRF in the no-variability ($q = 0$) and full-variability cases. The $q = 0$ curve corresponds to M, while the difference between the two curves is V, shown by the solid line in Fig. 5a. V peaks at $30°$ latitude, where it actually accounts for *all* of the cloud forcing. This region is at the boundary between the dry subtropics, essentially free of mid-level and high cloud, and the midlatitude storm tracks where clouds are plentiful. At higher latitudes, the variability contribution is very small. As shown by the dashed and dotted curves, this is due to a cancellation between longwave and shortwave components, which are large but of opposite sign.

The details of how this variability contribution comes about lie in the model parameterizations of the interactions of long- and shortwave radiation with the cloud field. We have examined this closely (Langen, 2005) but choose here, due to the model dependency, to merely summarize our conclusions. At all latitudes, the dominant vertical pattern of cloud variability is single-signed, i.e., low, medium and high cloud fractions tend to covary. The random-overlap assumption employed in the CCM3's longwave cloud parameterization has the consequence (which can be shown analytically) that single-signed variability yields lower vertically averaged total cloud cover than do fixed time-average clouds. This effect strengthens with the number of layers with cloud variability, and the overall picture of negative longwave contribution to V in Fig. 5a (dotted curve) is due to the decreased

cloud-greenhouse effect accompanying the decreased total cloud cover seen in Fig. 5b. The mid- and high latitudes have a thicker cloud deck and thus experience a larger effect.

In the shortwave part of the model's radiation code, overlap is parameterized by scaling the layer optical depth with the cloud fraction to the power $3/2$ (Briegleb, 1992). We find that this has the consequence that in a high-transmission mean atmosphere (e.g., with little cloudiness or small zenith angle) variability will give shortwave cooling, while conversely, variability in a low-transmission mean atmosphere will lead to warming. This is reflected in Fig. 5a (dashed curve) where the low latitudes, which have few cloudy layers and small zenith angles, experience a cooling effect. The mid- and high latitudes, with more cloudy layers and larger zenith angles, experience a warming, which weakens with latitude due to decreasing cloud water content.

4   Cloud variability and climate change

We saw above that a substantial part of the cloud forcing in the reference climate is due to cloud variability, and this forcing could be even larger were it not for a cancellation between the short- and longwave effects. How the forcing changes and whether such a cancellation continues to hold in a changed climate is not obvious. To address these issues, we perform a model integration identical in every respect to the reference run but employing quadrupled CO_2 concentration ("$4\times$" run). This run has a global-mean SST about $5\ °C$ higher than the reference run, which results in an elevated tropopause and hence greater upper-level mean cloudiness and variability (Fig. 6). There is also a $6°C$ reduction in equator-to-pole temperature difference, as well as a slight poleward shift and weakening of the midlatitude storm tracks, resulting in reduced mean cloudiness and variability in the lower troposphere, especially in midlatitudes. The horseshoe-shaped area of reduced cloud fraction variability is similar to the area of reduced ω-variability shown in Fig. 6c, a clear indicator of the reduction in the midlatitude eddy activity. In general, the $4\times$ run is associated with a reduced column-integrated cloudiness.

Our aim in this section is to assess the radiative impact of the cloud changes in Fig. 6. To do this, we again employ the cloud resampling method of Section 2. We output cloud data at 2 hour intervals from the $4\times$ run, and then perform fixed-SST runs with clouds specified by reading from this dataset. We emphasize that *all* fixed-SST runs here use SST and CO_2 values taken from the *reference* run, i.e., we use $4\times CO_2$ clouds with $1\times CO_2$ SSTs. Thus, changes in CRF are due solely to changes in clouds and not in clear-sky radiation[1]. Our method is thus closer to an offline radiation calculation than to the CRF approach of Cess and Potter

---

[1] With the small caveat that since temperature and humidity are internally calculated in the fixed-SST runs, it can be argued that cloud changes may drive changes in these fields that will bias the clear-sky radiation. However, this caveat applies only to the longwave component, and considering the very strong control that SST exerts on the climate, we expect the resulting bias to be small, on the order of the bias introduced by cloud decorrelation.
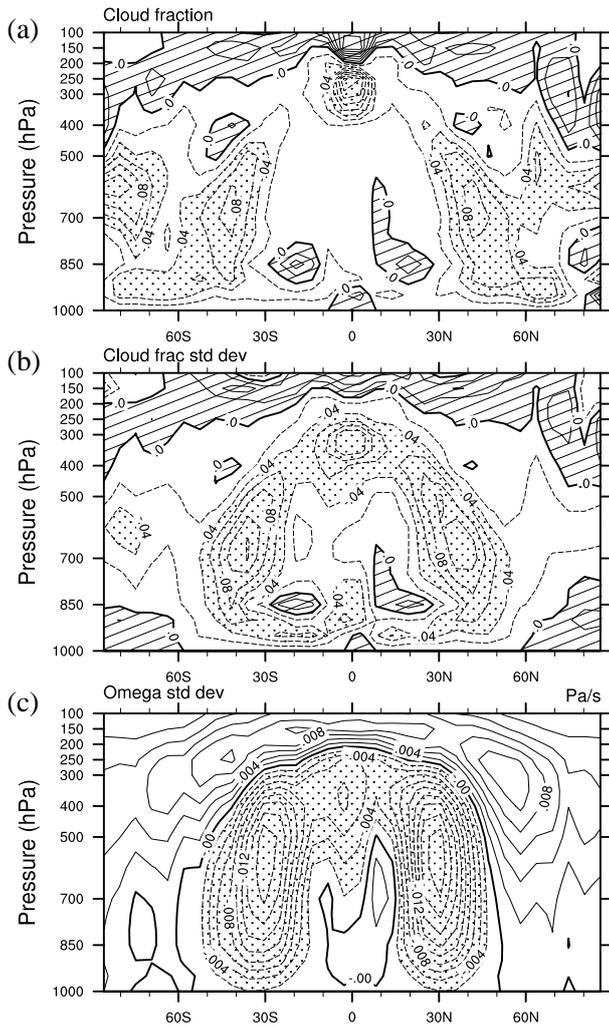
(a)

(b)

(c)

Figure 6. (a) Time- and zonal-mean change in cloud fraction due to quadrupling CO_2. (b) As in (a) but for standard deviation. (c) As in (a) but for vertical velocity standard deviation. To ease readability, negative contours are dashed and in panels (a) and (b) positive contours are hatched while contours less than -0.04 are stippled. In panel (c), contours less than -0.002 are stippled.

(1987). Using the notation of Eq. (1), we may formalize this as

$$\Delta \overline{CRF} = \overline{CRF}_4 - \overline{CRF}_1 \tag{3}$$

$$\Delta M = M_4 - M_1 \tag{4}$$

$$\Delta V = V_4 - V_1 = \Delta \overline{CRF} - \Delta M, \tag{5}$$

where $\overline{CRF}_4$ is time-mean CRF in the fixed-SST run employing fully-variable clouds ($q=1$) from the $4\times$ run, while M_4 is the same quantity for the case with fixed clouds ($q=0$). Index 1 indicates analogous quantities using clouds from the reference run.

Results are shown in Fig. 7a and summarized in Table 1. $\Delta \overline{CRF}$ is weakly negative in the tropics and strongly positive in the extratropics. This latitudinal structure of total cloud feedback contributes towards reduced meridional temperature gradients in the warmer climate, exacerbating the effects of dynamical heat transports (see Alexeev et al., 2005). ΔM gives the dominant contribution, but ΔV also

Table 1. Cloud radiative feedbacks (Eqs. (3)–(5)) averaged globally and over the tropics (30°S–30°N) and extratropics (90°S–30°S, 30°N–90°N). Units are W m^{-2}.

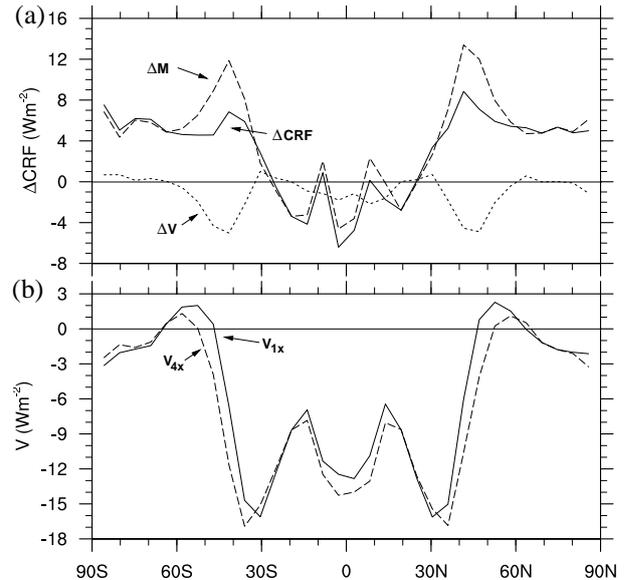|	Global	Trop	Ex-trop
$\Delta \overline{CRF}$	1.82	-1.92	5.55
ΔM	3.06	-1.19	7.32
ΔV	-1.25	-0.73	-1.77

(a)

(b)

Figure 7. (a) Cloud radiative feedbacks in the $4\times$ run: $\Delta \overline{CRF}$ (solid), ΔM (dashed) and ΔV (dotted). (b) V contributions in the $1\times$ (solid) and $4\times$ (dashed) runs. The ΔV in panel (a) is the difference between these two.

plays a significant role, offsetting much of the warming due to ΔM in the midlatitudes. Moreover, changes in cloud variability *reduce* the tendency to weaken the meridional temperature gradient in this experiment.

The reduction in V is closely related to changes in storm-track eddy activity: in the mid-latitudes, ω-variability decreases (Fig. 6c) and eddy kinetic energy density (not shown) drops by about 15%. These amplitude changes are accompanied by a poleward shift which in Fig. 7b is seen to influence the V change. As shown in Caballero and Langen (2005), storm track eddy activity may either weaken or intensify with global warming, depending on the details of the reference climate: in general, cooler climates (with global mean temperatures less than $\sim 15°$C) will show intensified storm tracks as they warm, while climates that are already warm will respond to further warming with a weakening of the storm tracks. In Caballero and Langen (2005), we speculate that the former is due to eddies being energized by latent heat release (as studied by Lapeyre and Held, 2004) while the latter is due to decreasing Eady growth rates accompanying increased static stability. Clearly, the particular case studied here falls in the latter category. However, the former category may be more appropriate for Earth's real climate: in a study of 15 GCMs used to simulate realistic 21st century global warming, Yin (2005) found a consistent increase in storm track intensity as the climate warmed. Thus cloud

variability could be influencing meridional temperature gradients in those simulations.

5   Discussion and conclusions

We have investigated the impact of cloud variability on the top-of-atmosphere radiative budget of NCAR's CCM3.6 GCM, run in an idealized aquaplanet configuration with no seasonality. Using a cloud resampling method, we found that the cloud variability contribution V accounts for 35% of global-mean CRF in the model's reference run. Geographically, V is highest in the midlatitudes and is related to cloud variability driven by extratropical eddy activity. A fourfold increase in CO_2 concentration resulted in a decrease and poleward shift of storm-track eddy activity and reduced V in mid-latitudes. Overall CRF change acts to reduce meridional temperature gradients in the warmer climate, but the change in V by itself tends to counter this effect.

The key conclusion of this paper is that changes in midlatitude eddy activity can, through their effect on cloud variability, strongly impact the radiative response of a GCM to greenhouse gas increase. In the experiments analyzed in this paper, the effect was due almost entirely to variability in cloud fraction, which brings into play the non-linearity in the cloud overlap scheme. Oreopoulos and Khairoutdinov (2003) studied cloud-scene snapshots from a cloud-resolving model and found that clouds spaced vertically by about 1 km were maximally overlapped, while clouds spaced by 5 km or more were randomly overlapped. Thus, some degree of random overlap seems inescapable, and this necessarily implies non-linearity (see Introduction). A wide variety of overlap schemes is used in current-generation GCMs (Barker et al., 2003); while the presence of some degree of non-linearity is a robust feature of such schemes, the details vary from scheme to scheme, and these differences will almost certainly have a large impact on V. In addition, two models sharing the same radiation and cloud overlap scheme but having different in storm track responses to climate change will also produce different values of V. Furthermore, there is no reason to think that the small role played by cloud water content variability in the present experiments is a robust feature. It is quite conceivable that a different cloud parameterization, or a different climate state, would give cloud water variability spanning the range over which non-linearity is important (see discussion in Introduction).

Overall, we conclude that V is likely to be a highly model-dependent quantity. Thus, much of the inter-model spread in cloud radiative feedbacks (e.g. Soden and Held, 2006; Webb et al., 2006; Ringer et al., 2006) may be due to differences in V. To underscore this point quantitatively, we can compute cloud feedback parameters for the present experiment, defined in the standard way (Bony et al., 2006) as $\lambda_x = \partial R_x/\partial T_s \approx \Delta R_x/\Delta T_s$, where ΔT_s is the change is global-mean surface temperature and ΔR_x is the resulting change in global-mean top-of-atmosphere radiative flux due solely to changes in variable x. Using the globally integrated values of $\overline{\Delta CRF}$, ΔM and ΔV given in Table 1 and ΔT_s=5 K, we find an overall cloud feedback λ_{CRF}=0.36 W m^{-2} K^{-1}, while the feedback due to change in mean clouds is λ_M=0.62 W m^{-2} K^{-1}; the difference is due to the negative cloud variability feedback, λ_V =-0.25 W m^{-2} K^{-1}.

A recent study (Soden and Held, 2006, their Fig. 1) shows that cloud feedback parameters in the IPCC AR4 (CMIP3) models range from 0.14 to 1.2 W m^{-2} K^{-1}. Thus, the role of V in the present model is to bring cloud sensitivity from the middle to the bottom of this range.

This paper does not aim at comprehensiveness, but instead is meant as a pilot study aimed at drawing attention to this somewhat overlooked aspect and to spurring further research into it. Specifically, we suggest two directions for future work. Firstly, it would be of obvious interest to quantify and intercompare V among a range of current GCMs run under given climate conditions and under standard climate change experiments. The cloud resampling methodology used here is simple and should be straightforward to implement in any GCM. Secondly, and perhaps of even greater importance, is the question of quantifying V for the real climate system directly from observations. It may be possible to do this using a combination of cloud amount data from the International Cloud Climatology Project (IS-CCP, Rossow and Schiffer, 1991) and top-of-atmosphere radiative fluxes from the Earth Radiation Budget Experiment (ERBE, Barkstrom, 1984). For example, one could compare the time-mean CRF over a given area with the CRF computed for individual snapshots in which the cloud distribution happens to be close to the time-mean distribution. Though it may be difficult to find a statistically significant number of such analogs, this approach would be of great interest as it avoids all recourse to a radiation model and its attendant parameterization issues.

The very simple boundary conditions employed here obviously limit the direct applicability of the results to the real climate system. They were, nevertheless, used to isolate cloud effects from those of, for example, sea ice and geography and to complement our earlier work on energy transports and meridional temperature gradients in the same simple setting (Alexeev et al., 2005; Caballero and Langen, 2005). The SW shielding effect by clouds is reduced over high-albedo surfaces such as ice and snow and including these would thus likely reduce the role played by the SW component of V in the reference climate. This would, in turn, shift the cancellation between the LW and SW effects at high latitudes in Fig. 5a and lead to an increased net cooling effect by V. In a climate warming experiment, melting sea ice would increase the shielding effect and thereby possibly negate some of the increase in high-latitude CRF change encountered in Fig. 7a. If seasons were included, the SW shielding would only be active during summer when the sun rises over the horizon. Thus, depending on the seasonality of both mean cloud and variability, the high-latitude cancellation between SW and LW would encounter large shifts over the seasons. Inclusion of realistic geography would not only produce hemispheric and zonal asymmetries in the cloud mean and variability and surface albedo; it would also enhance the tendency of seasonality and sea ice to create seasonal changes in mean temperature, meridional temperature gradients and thereby storminess. Such changes were in Section 4 seen to alter the role played by V relative to M.

As a final point, our results highlight an inconsistency often encountered in the cloud-radiation literature. As noted in the Introduction, the non-linear nature of cloud-radiation interaction is well known, and all studies of CRF go to great lengths to include cloud variability in their calcula-

tions. However, when it comes to *interpreting* these calculations and attributing changes in CRF to changes in clouds, it is very common to refer only to changes in mean cloud properties, ignoring changes in variability (e.g., Le Treut et al., 1994; Zhang et al., 1994; Colman et al., 2001; Webb et al., 2006; Ringer et al., 2006). However, as is apparent when comparing M and V in the reference climate (Fig. 4b (solid) and Fig. 5a (solid)) and the changes in M and V during climate change (Fig. 7a), the implicit assumption that changes in V are negligible or perhaps linearly related to M can be misleading. In fact, V was found to be of the same sign as M in the reference climate and account for 35% of the total CRF, while in the climate change experiment, its change was of the opposite sign and countered 40% of the CRF change due to M. Thus, ignoring the V contribution can be misleading. For example, while it may be possible to tune the radiation/cloud parameterization suite in a GCM so that it gives a reasonably realistic CRF in a reference climate, the results will likely be wrong in a changed climate with a different partitioning of M and V.

6   Acknowledgments

REFERENCES

Alexeev, V. A. (2003). Sensitivity to CO_2 doubling of an atmospheric GCM coupled to an oceanic mixed layer: a linear analysis. *Clim. Dyn.*, 20:775–787.

Alexeev, V. A., Langen, P. L., and Bates, J. R. (2005). Polar amplification of surface warming on an aquaplanet in "ghost forcing" experiments without sea ice feedbacks. *Clim. Dyn.*, doi:10.1007/s00382-005-0018-3.

Barker, H. W., Stephens, G. L., Partain, P. T., Bergman, J. W., Bonnel, B., Campana, K., Clothiaux, E. E., Clough, S., Cusack, S., Delamere, J., Edwards, J., Evans, K. F., Fouquart, Y., Freidenreich, S., Galin, V., Hou, Y., Kato, S., Li, J., Mlawer, E., Morcrette, J.-J., O'Hirok, W., Räisänen, P., Ramaswamy, V., Ritter, B., Rozanov, E., Schlesinger, M., Shibata, K., Sporyshev, P., Sun, Z., Wendisch, M., Wood, N., and Yang, F. (2003). Assessing 1D Atmospheric Solar Radiative Transfer Models: Interpretation and Handling of Unresolved Clouds. *Journal of Climate*, 16:2676–2699.

Barkstrom, B. R. (1984). The Earth Radiation Budget Experiment (ERBE). *Bull. Amer. Meteor. Soc.*, 65:1170–1185.

Bergman, J. W. and Salby, M. L. (1997). The Role of Cloud Diurnal Variations in the Time-Mean Energy Budget. *J. Climate*, 10:1114–1124.

Bony, S., Colman, R., Kattsov, V. M., Allan, R. P., Bretherton, C. S., Dufresne, J.-L., Hall, A., Hallegatte, S., Holland, M. M., Ingram, W., Randall, D. A., Soden, B. J., Tselioudis, G., and Webb, M. J. (2006). How well do we understand and evaluate climate change feedback processes? *J. Climate*, 19:3445–3482.

Briegleb, B. P. (1992). Delta-eddington approximation for solar radiation in the NCAR Community Climate Model. *J. Geophys. Res.*, 97(D7):7603–7612.

Caballero, R. and Langen, P. L. (2005). The dynamic range of poleward energy transport in an atmospheric general circulation model. *Geophys. Res. Lett.*, 32:L02705, doi:10.1029/2004GL021581.

Cess, R. D., Genio, A. D., Dix, M., Esch, M., Fowler, L., Fraser, J., Galin, V., Gates, W., Hack, J., Kiehl, J., Treut, H. L., Zhang, M., Lo, K., McAvaney, B., Meleshko, V., Morcrette, J., Randall, D., Roeckner, E., Royer, J., Schlesinger, M., Sporyshev, P., Timbal, B., Ingram, W., Volodin, E., Taylor, K., Wang, W., Wetherald, R., Potter, G., Alekseev, V., Barker, H., Cohen-Solal, E., Colman, R., and Dazlich, D. (1996). Cloud feedback in atmospheric general circulation models: An update. *J. Geophys. Res.*, 101D:12791–12794.

Cess, R. D. and Potter, G. L. (1987). Exploratory studies of cloud radiative forcing with a general circulation model. *Tellus* 39A:460–473.

Collins, W. D. (2001). Parameterization of generalized cloud overlap for radiative calculations in general circulation models. *J. Atmos. Sci.*, 58:3224–3242.

Colman, R., Fraser, J., and Rotstayn, L. (2001). Climate feedbacks in a general circulation model incorporating prognostic clouds. *Clim. Dyn.*, 18:103–122.

Geleyn, J. F., and Hollingsworth, A. (1979). An economical analytical method for the computation of the interaction between scattering and line absorption of radiation. *Contrib. Atmos. Phys.*, 52:115.

Harshvardhan and Randall, D. A. (1985). Comments on "The parameterization of radiation for numerical weather prediction and climate models". *Mon. Wea. Rev.*, 113:1832–1833.

Houghton, J. T., Ding, Y., Griggs, D. J., Noguer, M., van der Linden, P. J., and D. Xiaosu, *Eds.* (2001). *IPCC, Climate Change 2001: The Scientific Basis.* Cambridge University Press, 944pp.

Kiehl, J. T., Hack, J. J., Bonan, G. B., Boville, B. A., Briegleb, B. P., Williamson, D. L., and Rasch, P. J. (1996). Description of the NCAR Community Climate Model (CCM3). Technical Report TN-420, CGD, National Center for Atmospheric Research.

Langen, P. L. (2005). *Polar amplification of surface temperature change in a warming climate.* PhD thesis, Niels Bohr Institute, University of Copenhagen, Denmark.

Langen, P. L. and Alexeev, V. A. (2004). Multiple equilibria and asymmetric climates in the CCM3 coupled to an oceanic mixed layer with thermodynamic sea ice. *Geophys. Res. Lett.*, 31:doi: 10.1029/2003GL019039.

Lapeyre, G. and Held, I. M. (2004). The role of moisture in the dynamics and energetics of turbulent baroclinic eddies. *J. Atmos. Sci.*, 61:1693–1710.

Le Treut, H., Li, Z. X., and Forichon, M. (1994). Sensitivity of the LMD General Circulation Model to Greenhouse Forcing Associated with Two Different Cloud Water Parameterizations. *J. Climate*, 7:1827–1841.

Oreopoulos, L. and Khairoutdinov, M. (2003). Overlap properties of clouds generated by a cloud-resolving model. *J. Geophys. Res.*, 108:doi:10.1029/2002JD003329.

Ramanathan, V., Cess, R. D., Harrison, E. F., Minnis, P., Barkstrom, B. R., Ahmad, E., and Hartmann, D. (1989). Cloud-radiative forcing and climate: Results from the earth radiation budget experiment. *Science*, 243:57–63.

Randall, D., Khairoutdinov, M., Arakawa, A., and Grabowski, W. (2003). Breaking the cloud parameterization deadlock. *Bull. Amer. Meteor. Soc.*, 84:1547–1564.

Ringer, M. A., B. J. McAvaney, N. Andronova, L. E. Buja, M. Esch, W. J. Ingram, B. Li, J. Quaas, E. Roeckner, C. A. Senior, B. J. Soden, E. M. Volodin, M. J. Webb

and K. D. Williams (2006). Global mean cloud feedbacks in idealized climate change experiments 33:L07718, doi:10.1029/2005GL025370.

Rossow, W. B. and Schiffer, R. A. (1991). ISCCP cloud data products. *Bull. Am. Met. Soc.*, 72:2–20.

Schneider, E. K., Kirtman, B. P., and Lindzen, R. S. (1999). Tropospheric water vapor and climate sensitivity. *J. Atmos. Sci.*, 56:1649–1658.

Sloan, L. C. and Pollard, D. (1998). Polar stratospheric clouds: A high latitude warming mechanism in an ancient greenhouse world. *Geophys. Res. Lett.*, 25:3517–3520.

Soden, B. J., Broccoli, A. J., and Hemler, R. S. (2004). On the use of cloud forcing to estimate cloud feedback. *J. Climate*, 17:3661–3665.

Soden, B. J. and Held, I. M. (2006). An assessment of climate feedbacks in coupled oceanatmosphere models. *J. Climate*, 19:3354–3360.

Stephens, G. L. (2005). Cloud feedbacks in the climate system: A critical review. *J. Climate*, 18:237–273.

Stephens, G. L., Wood, N. B., and Gabriel, P. M. (2004). An assessment of the parameterization of subgrid-scale cloud effects on radiative transfer. part I: Vertical overlap. *J. Atmos. Sci.*, 61:715–732.

Taylor, K. E. and Ghan, S. J. (1992). An analysis of cloud liquid water feedback and global climate sensitivity in a general circulation model. *J. Climate*, 5:907–919.

Vavrus, S. J. (2004). The impact of cloud feedbacks on arctic climate under greenhouse forcing. *J. Climate*, 17:603–615.

Manabe, S. and Strickler, R. F. (1964). Thermal equilibrium of the atmosphere with a convective adjustment. *J. Atmos. Sci.*, 21:361–385.

Wetherald, R. T. and Manabe, S. (1988). Cloud feedback processes in a general circulation model. *J. Atmos. Sci.*, 45:1397–1415.

Yin, J. H. (2005). A consistent poleward shift of the storm tracks in simulations of 21st century climate. *Geophys. Res. Lett.*, 32.

Webb, M. J. and Senior, C. A. and Sexton, D. M. H. and Ingram, W. J. and Williams, K. D. and Ringer, M. A. and McAvaney, B. J. and Colman, R. and Soden, B. J. and Gudgel, R. and Knutson, T. and Emori, S. and Ogura, T. and Tsushima, Y. and Andronova, N. and Li, B. and Musat, I. and Bony, S. and Taylor, K. E. (2006). On the contribution of local feedback mechanisms to the range of climate sensitivity in two GCM ensembles. *Climate Dynamics*, 27:17–38.

Zhang, M. H., Hack, J. J., Kiehl, J. T., and Cess, R. D. (1994). Diagnostic study of climate feedback processes in atmospheric general circulation models. *J. Geophys. Res.*, 99(18):5525–5538.